Published in final edited form as:
Bioconjug Chem. 2010 May 19; 21(5): 828–835. doi:10.1021/bc9005317.

Hexylether Derivative of Pyropheophorbide-a (HPPH) on Conjugating with 3Gadolinium(III) Aminobenzyldiethylenetriaminepentaacetic Acid Shows Potential for *In vivo* Tumor-Imaging (MR, Fluorescence) and Photodynamic Therapy

Joseph A. Spernyak[1], **William H. White III**[2], **Manivannan Ethirajan**[2], **Nayan J. Patel**[2,3], **Lalit Goswami**[2], **Yihui Chen**[2], **Steven Turowski**[1], **Joseph. R. Missert**[2], **Carrie Batt**[2], **Richard Mazurchuk**[1], and **Ravindra K. Pandey**[2]

[1] Preclinical Imaging Facility, Roswell Park Cancer Institute, Buffalo, NY 14263

[2] PDT Center, Cell Stress Biology, Roswell Park Cancer Institute, Buffalo, NY 14263

[3] Molecular Pharmacology and Cancer Therapeutics, Roswell Park Cancer Institute, Buffalo, NY 14263

Abstract

Conjugates of 3-(1′-hexyloxyethyl)-3-devinyl pyropheophorbide-a (HPPH) with multiple Gd(III) aminobenzyl diethylenetriamine pentacetic acid (ADTPA) moieties were evaluated for tumor imaging and photodynamic therapy (PDT). *In vivo* studies performed in both mice and rat tumor models resulted in a significant MR signal enhancement of tumors relative to surrounding tissues at 24h post-injection. The water soluble (pH: 7.4) HPPH-3Gd(III) ADTPA conjugate demonstrated high potential for tumor imaging by MR and fluorescence. This agent also produced long-term tumor cures *via* PDT. An *in vivo* biodistribution study with the corresponding ^{14}C-analog also showed significant tumor-uptake 24 hours post-injection. Toxicological evaluations of HPHH-3Gd(III) ADTPA administered at and above imaging/therapeutic doses did not show any evidence of organ toxicity. Our present study illustrates a novel approach for the development of water soluble "multifunctional agents", demonstrating efficacy for tumor imaging (MR and fluorescence) and phototherapy.

INTRODUCTION

Early detection and treatment of cancer presents numerous clinical benefits. While the disease is well-localized and neoplastic growths are small, highly localized therapies have the potential advantage of reduced side-effects and minimal damage to normal tissues (as opposed to systemic chemotherapy or invasive surgery). One example of localized therapy is photodynamic therapy, or PDT. PDT works *via* the creation of cytotoxic singlet oxygen formed by exposing a photosensitizing agent with an appropriate wavelength of a laser light (1).

One of the first photosensitizing agents approved for treatment of cancer is porfimir sodium (Photofrin®). Photofrin® isconsidered a first-generation photosensitizer and has been used in

Supporting Information Available: *In vivo* MR images of conjugates **1–5** and the intracellular localization of HPPH-3Gd(III)aminobenzyl DTPA **3**.

the treatment of Barrett's esophagus (2) cervical cancer (3), endobronchial cancer (4), and papillary bladder cancer (5). However, Photofrin® has several inherent limitations, namely its low molar absorption coefficient (1,170 $M^{-1}cm^{-1}$) (6) as well as skin photosensitivity resulting from residual photosensitizer delocalized throughout the skin (7). These limitations have led to the development of "second generation" sensitizers which absorb energy efficiently at longer wavelengths and localize more effectively within the tumor. One such compound is 3-[1′-hexyloxyethyl]-3-devinyl pyropheophorbide-*a* (HPPH), which has a peak absorbance at 665 nm (*in vivo* absorption) and is currently in phase II clinical trials for the treatment of esophageal, lung, and cutaneous tumors (8,9). In contrast to most porphyrin-based agents, HPPH does not show any significant skin phototoxicity in the patients.

A typical treatment regimen involves the single injection of agent followed by light illumination of the tumor after time has passed to allow for tumor uptake of the PDT agent. As PDT requires direct illumination of light onto the photosensitizer, image-guided therapy may be an effective way to efficiently a) determine the size and extent of the tumor and b) assist the clinician in localizing the light source onto the tumor. While still relatively novel in application, image-guided PDT has shown efficacy as a primary treatment in head and neck cancer (10) or as an adjuvant treatment to fluorescence guided resection in high grade gliomas (11) and melanomas that have metastasized to the brain (12). To this end, we have explored the feasibility of incorporating imaging functionality into porphyrin-based PDT agents to develop compounds that can be used in both diagnosis and therapy.

Magnetic resonance imaging (MRI) is well-suited for image guided therapy, as it does not require ionizing radiation, is non-invasive, and provides three-dimensional tomographic datasets with excellent soft tissue contrast. Use of gadolinium-based contrast agents have shown utility in the diagnosis of cancer (13–16) and in the study of numerous other disease states (17,18). Gadolinium, or Gd(III), has seven-unpaired electrons within inner orbital shells, giving it a high degree of paramagnetism, which causes an increase in the T_1 relaxation rates (R_1) of nearby water molecules, thereby enhancing the MR signal.

Magnetic resonance imaging has numerous limitations, however. Detection sensitivity of MR contrast agents is relatively poor, requiring levels of Gd(III) to be at micromolar concentrations within the tissues. Determination of the degree of tissue signal enhancement requires comparison of pre-injection and post-injection images. In comparison to contrast-enhanced MRI, fluorescence imaging has a much higher sensitivity in the detection of imaging agents and does not require multiple imaging time points. Fluorescence imaging is relatively inexpensive and can be employed in situations where MRI is ill-suited for use, such as such imaging subjects with metal embedded within their bodies or who cannot remain motionless. Therefore, incorporating both optical and MR imaging functionality into an effective photosensitizer allows one to incorporate the complementary strengths of each imaging modality.

Previously, we reported on the utility of tumor-avid HPPH in developing "multifunctional agents" (19) where HPPH was conjugated with Gd (III)-DTPA and showed *in vivo* tumor enhancement at 24h post-injection on MR images. However, due to its low water solubility it was difficult to formulate at higher concentrations.

In this report, we describe the comparative *in vivo* tumor imaging and PDT efficacy of a series of conjugates containing 3- or 6-Gd(III)aminobenzyl DTPA units with the expectation that the additional number of Gd(III) units would improve solubility and increase tumor conspicuity. Among the compounds evaluated, the HPPH-3 Gd(III)aminobenzyl DTPA was selected as a lead compound on the basis of its imaging potential, *in vitro* PDT efficacy, and ease of synthesis. The utility of the conjugate was further evaluated for *in vivo* fluorescence imaging,

in vivo PDT efficacy, organ toxicity, and PDT-induced mechanism of action. In addition, an *in vivo* biodistribution study of the lead conjugate was performed with the corresponding ^{14}C-labeled analog.

EXPERIMENTAL PROCEEDURES

Chemistry

A detailed report on the synthesis, characterization, *in vitro* intracellular localization and T_1 relaxivity of the multifunctional agents is reported in our preceding publication of this journal. In brief, three groups of compounds were synthesized (Figure 1): (i) HPPH with 3- or 6 Gd (III)- aminobenzylDTPA, (ii) Pyro-based photosensitizer with 3- or 6 Gd(III)-aminobenzylDTPA groups in which the hexyl chain of HPPH is replaced with an ether-linked triethyleneglycol functionality (OTEG) (iii) a purpurinimide analog [longer wavelength photosensitizer (λ_{max}: 700 nm)] linked with 3 Gd(III)-aminobenzylDTPA. Although all the conjugates showed potential for tumor imaging (MRI), HPPH conjugated with 3Gd(III) ADTPA (Figure 1) was found to be most promising as multifunctional agent for tumor imaging and phototherapy, and therefore was investigated further for detailed biological evaluation.

Selection Criteria of the best candidate for tumor- imaging and PDT—In our preceding paper we have discussed the synthesis, photophysical characteristics, *in vitro* T_1/T_2 MR relaxivity, and *in vitro/in vivo* PDT efficacy of a series of HPPH-Gd(III)ADTPA conjugates. Some of the analogs showed enhanced tumor contrast, but limited PDT efficacy. Because the objective of our research was focused on developing “Multifunctional Agents” for tumor-imaging and phototherapy, we selected only those candidates which showed both imaging and therapeutic potential. The selection criteria we used for identification of the lead compound are summarized in Figure 2.

Synthesis of ^{14}C-labeled HPPH aminotriester derivative 7—^{14}C-HPPH 6 (15.0 mg, 0.023 mmol; specific activity: 5.2 μCi/μmol), aminotriester (15 mg, 0.036 mmol), EDCI (1-Ethyl-3-(3-dimethylaminopropyl)carbodiimide hydrochloride); (9 mg, 0.05 mmol) and DMAP (4-dimethylaminopyridine); (6 mg, 0.05 mmol) were taken in a dry round bottom flask (25 ml). Dry dichloromethane (DCM, 5 ml) was added and reaction mixture was stirred at room temperature (RT) for 12 hr under N_2 atm. Reaction mixture was diluted with DCM (10 ml), washed with brine solution, organic layer separated, dried over sodium sulfate and concentrated. Crude mixture was purified over preparative thin layer chromatography (silica gel) using 1% MeOH/DCM mixture to give the desired product **7**. Yield: 18.0 mg (76.0%).

Synthesis of ^{14}C-labeled HPPH tri-AminobenzylDTPA ester 8—Compound **7** (17.0 mg, 0.016 mmol) was stirred with 70% trifluoroacetic acid (TFA)/DCM (2.0 ml) at room temperature for 5 hr. Resultant mixture was concentrated and dried under high vacuum to remove trace TFA. To this crude were added, amino-benzyl-DTPA-penta-*tert*-butyl ester (54.0 mg, 0.069 mmol), EDCI (20.0 mg, 0.103 mmol) and DMAP (12.0 mg, 0.103 mmol). Dry dichloromethane (5 ml) was added and reaction mixture was stirred at RT for 16 hr under N_2 atm. Reaction mixture was further diluted with dichloromethane (10 ml), washed with brine solution, organic layer separated, dried over sodium sulfate and concentrated. Crude mixture was purified over short column (0.5 cm width, 12 cm height) containing Grade-III alumina as a stationary phase and a 3% MeOH/DCM mixture as eluent to give product **8**. Yield (2 steps): 31.0 mg (61.0%).

Synthesis of ^{14}C-labeled HPPH 3Gd(III)-AminobenzylDTPA complex 9—Compound **8** (30.0 mg, 0.009 mmol) was stirred with 70% TFA/DCM (2.0 ml) at RT for 5 hr. Resultant mixture was concentrated and dried under high vacuum to remove trace TFA. The

crude obtained was dissolved in pyridine (2 ml) and put under continuous stirring. $GdCl_3.6H_2O$ (20.0 mg, 0.054 mmol) in 0.5 ml of water was slowly added to this solution and resultant mixture was stirred for an additional 16 hr. Reaction mixture was filtered and the residue obtained was washed with water (10 ml × 3), acetone (10 ml × 3) and then dried under high vacuum to yield gadolinium complex **9**. Yield: 18.0 mg (72.0%). Specific activity: 3.9 μCi/mol.

Animal Models—*In vivo* PDT experiments were performed in two tumor models, C3H mice bearing radiation induced fibroblast (RIF) tumors and BALB/c mice bearing Colon 26 tumors (NCI, Bethesda, MD). These tumor models were chosen as they have been extensively characterized in our lab in determining the PDT efficacy of numerous photosensitizers. In both models, tumor cells (1×10^6 Colon 26 cells in 50 μL PBS, 4×10^5 RIF cells in 50 μL PBS) were implanted subcutaneously and were allowed to grow to an approximate diameter of 5–7 mm. For MR imaging of the most promising candidates, Ward tumor cells were implanted subcutaneously above the intraperitoneal cavity of adolescent Fischer 344 rats (Harlan Laboratories) (150–200 g). Tumors were allowed to grow to ~1cm in diameter prior to MR imaging. The *in vivo* biodistribution of the ^{14}C-labeled lead compound was also performed in rats bearing Ward tumors. Due to the size limitation of the *in vivo* fluorescence instrument, the fluorescence imaging of the lead compound was performed in BALB/c mice bearing Colon 26 tumors. All animal procedures were carried out in accordance to guidelines approved by the Institute Animal Use and Care Committee.

MR imaging potential of the conjugates—Among the compounds investigated, the conjugates containing three Gd(III)ADTPA moieties had better *in vitro* PDT activity than those containing six Gd(III)ADTPA (see the preceding paper in this Journal). Therefore, only those conjugates bearing three Gd(III)ADTPA chelates were examined for detailed *in vivo* MR imaging ability (tumor contrast enhancement) in rats bearing Ward tumors. Prior to imaging, anesthesia was induced in the animals with 4% isoflurane and maintained with 2% isoflurane during imaging. Animal temperature and respiration rate were monitored with an MR-compatible small animal monitoring system (Model 1025, SAII, Stony Brook, NY), and temperature was maintained at 32° C with warm air. A sealed tube containing 150 μM Gd(III)-DTPA (Magnevist®, Bayer HealthCare Pharmaceuticals) was placed on each side of each animal to serve as an MR signal intensity calibration standard.

Prior to tail vein administration of each agent (dose:10 μmol/kg), MRI data sets were acquired for each animal to serve as baseline controls, and then animals were re-scanned 24 hours after injection. An additional MRI data set was acquired at 8 hours post injection of conjugate **2** (Pyro-OTEG-3Gd) because a faster clearance rate from the body was anticipated. For comparison to clinically administered MRI contrast agents, two separate groups of rats (n=3 per group) were imaged immediately before and after the administration of Gd(III)-DTPA *via* tail-vein catheter at the clinically recommended dose of 100 μmol/kg, as well as at 10 μmol/kg to compare imaging results with our multifunctional agents.

Two SE imaging protocols were used with identical slice prescription parameters [5–6 axial slices, 1.5 mm slice thickness, 6×6 cm FOV(field of view), 256×192 acquisition matrix zero-filled to 256×256]. First, a moderately T_1-weighted scan acquired with a TE/TR of 10/1200 ms (echo and repetition time, respectively), and second, a heavily T_1-weighted scan acquired with Chemical Shift Selective (CHESS) fat suppression with a TE/TR of 10/356 ms.

Additionally, T_1 relaxation rates for tissues were determined by acquiring a series of 6 fast spin echo-encoded scans with TR's ranging from 360 to 6000 ms.

Lastly, *in vivo* testing of HPPH-3Gd(III)ADTPA was performed with an orthotopic RIF tumor model implanted into the thigh muscle of C57bl/6 mice. Imaging parameters were modified to achieve higher resolution required for imaging mice (FOV = 32 mm, matrix size = 160×160, slice thickness = 1mm). All other data acquisition parameters were identical to the MR imaging protocol described above.

In vivo MR data sets were processed with commercially available software (Analyze 7.0, Analyze Direct, Overland Park, KS) by defining a region of interest (ROI) for tumor, muscle surrounding the backbone, and the 150 μM Gd-DTPA calibration standards. Following segmentation, the mean signal intensities for each ROI were sampled. To normalize signal intensity values acquired at different time points, all signal intensity values were divided by the average intensity value of the two Gd-DTPA phantoms. Normalized contrast between tumor and muscle was then determined by subtraction of the mean signal intensity of the two regions. T_1 relaxation rates of tumor and back muscle were calculated by taking the mean intensity within ROI's, and R_1 and S_{MAX} were calculated by nonlinear fitting of the equation:

$$S_{(TR)}=S_{MAX}(1-e^{-(R1*TR)})+\text{Background Noise}$$

using Matlab's Curve Fitting Toolbox (Matlab 7.0, MathWorks Inc., Natick, MA). Tissue concentrations of agents were estimated using the following equation:

$$[CA]=(R1_{post-inj}-R1_{pre-inj})\div\text{Relaxivity},$$

where the compound relaxivity was determined and reported in the accompanying paper.

Fluorescence Imaging—Fluorescence imaging of photosensitizer accumulation in the tumor was carried out using a Nuance™ optical imaging camera system (Cambridge Research Inc, Woburn, MA). When the tumor reached 4–5 mm in diameter, mice were anesthetized with either a ketamine/xylene mixture (100/10 mg/kg) or 8 mg/kg of pentobarbitol sodium. Prior to imaging, Nair® was used to remove hair from the skin surrounding the Colon 26 tumors. Fluorescent excitation was achieved using a spectrum between 525–555 nm using a tungsten-halogen light source. Spectral emission images were acquired from a range of 550–700 nm prior to and 24 hours post-administration of HPPH-3Gd(III)ADTPA. HPPH-specific images were spectrally unmixed using the Nuance™ software and represented in false color images.

In vivo PDT efficacy and assessment of response—When tumor reached 4–5 mm in diameter, the mice were injected with HPPH-3Gd(III)ADTPA at the imaging dose (10 μmol/kg). Prior to PDT treatment, Nair® was used to remove all hair surrounding the tumor site. At 24 h post- injection, the mice were restrained in plastic plexiglass holders without anesthesia, treated with a laser light (70 J/cm^2, 70 mW/cm^2). Following treatment, mice were observed daily for tumor re-growth or tumor cure. Visible tumors were measured using two orthogonal measurements, L and W (L perpendicular to W) and the volumes were calculated using the Microsoft Excel formula V = L*W^2/2 and recorded. Mice were considered cured if there was no palpable tumor by day 60. Mice were euthanized if the tumor reached 400 mm^3 due to tumor burden.

In vivo biodistribution studies

The ^{14}C-labeled photosensitizers (0.2 mL/0.08μCi) were individually administered to mice through a lateral tail vein [3 mice/group (BALB/c mice bearing Colon 26 tumors and C3H mice bearing RIF tumors)]. At 24 and 48 hours post-injection, 3 mice per time point were sacrificed by CO_2 asphyxiation. The blood was collected into heparinized syringes and

immediately centrifuged to obtain plasma. The plasma was transferred to a scintillation vial for ^{14}C counting. The organs of interest (skin, muscle, tumor, heart, lung, liver, kidney and spleen) were removed. Sample weights were recorded and 1 ml of Solvable™ (PerkinElmer, Waltham, Massachusetts) was added to each sample and incubated overnight at 53°C. The samples were allowed to dissolve before adding 80 μl of peroxide (20 μl at a time). After samples were sufficiently bleached, 15 ml of scintillation fluid was added and the samples were run on a Beckman LS 6000LL scintillation counter. Raw data were then converted to counts per gram tissue weight and plotted using SigmaPlot 10.0 software.

Toxicological Study—To assess the possible toxicity effects of our lead imaging agent, HPPH-3Gd(III)ADTPA was injected into 27 rats (9 rats/group) at concentrations of 5 μmol/kg (lower than the imaging dose), 10 μmol/kg (imaging dose) and 25 μmol/kg (higher than the imaging dose). An additional 3 rats were used as control. Animals were sacrificed 14 days post-injection; liver, spleen, kidney, skin, heart and lung were collected and fixed in formalin. Fixed tissue specimens were embedded in paraffin, sectioned, and subsequently stained with hematoxylin and eosin (H&E). Individual tissue sections were examined by light-field microscopy for evidence of toxicity.

RESULTS

^{14}C-labeled HPPH-3GD(III)-DTPA 9

The ^{14}C-labeled HPPH was synthesized from methyl pyropheophorbide-a by following the reported procedure. It was then converted into the corresponding 3Gd(III)-ADTPA (specific activity: 3.9 μCi/μmol) analog by following the methodology reported for the non-labeled conjugate in our preceding paper in this Journal.

In vivo tumor enhancement by MR imaging—All HPPH-Gd(III) ADTPA conjugates containing either 3- or 6 gadolinium units showed tumor contrast enhancement 24 hours after administration. However, our objective was to develop dual-function agents which could be used for both tumor-imaging and therapy. Unfortunately, the conjugates with six gadolinium units showed limited photosensitizing efficacy. Therefore only those conjugates containing 3 Gd(III)-ADTPA groups were investigated for *in vivo* assessment of tumor contrast enhancement. Figure 3 shows the increase in the normalized contrast between tumor and muscle at 24 hours post injection of each of the 3Gd(III)-ADTPA containing agents (Pyro-OTEG-3Gd(III)ADTPA was also imaged at 8 hours post injection).

All of the multifunctional agents showed increased tumor-to-muscle contrast as compared to baseline values. HPPH-3Gd(III)ADTPA showed the greatest increase in tumor conspicuity in both T_1-weighted scans. As a result, HPPH-3Gd(III)ADTPA was selected for further characterization at lower doses and in an additional tumor model.

HPPH-3Gd(III)ADTPA also showed quantifiable increases in tumor to muscle contrast and T_1 relaxation rates at 5 and 2.5 μmol/kg, albeit lower than the increases from the 10 μmol/kg dose. Percent increases in tumor to muscle contrast from baseline values for each dose are shown in Table 1, as well as the average increase in T_1 relaxation rate of the tumor. At administered doses of 10 and 5 μmol/kg of HPPH-3Gd(III)ADTPA, the increase in tumor signal intensity could be seen clearly (Figure 4). However, at a dose of 2.5 μmols/kg, tumor signal enhancement was not discernable visually (not shown). T_1 relaxometry of tumor and muscle before and after injection showed preferential tumor uptake of all of the 3Gd(III) ADTPA conjugates tested (Figure 5). Only minimal increases in T_1 relaxation rates compared to baseline values were observed in normal tissue (muscle) 24 hours after injection. Tumor specific enhancement by HPPH-3Gd(III)ADTPA was also seen in an orthotopic RIF tumor model. A significant increase in contrast between tumor and adjacent leg muscle was exhibited

(Figure 6). Contrast between tumor and leg muscle increased an average of 36% for the two scan protocols employed.

In vivo fluorescence imaging—Fluorescence imaging potential of HPPH-3Gd(III) ADTPA was evaluated at the imaging dose (10 μmol/kg) in BALB/c mice bearing Colon26 tumors at 24, 48, and 72h post-injection. The fluorescence intensity measured in the tumor was maximum at the 24 h postinjection, but was still visible at 48 h. At 72 h the majority of the drug has washed out leaving only minimal fluorescence. Tumor enhancement was highest in the 24 hour image with a tumor to skin intensity ratio of3.79 compared with only 2.73 at 48 hours (Figure 7).

In vivo PDT efficacy—For *in vivo* screening, 6Gd(III)ADTPA-HPPH conjugate **4** which showed the best T1 and T2 relaxivity was initially evaluated at variable doses (2.5, 5.0 and 10.0 μmol/kg) in mice bearing RIF tumors.

Tumors were exposed to a laser light (135 J/cm ^{2}, 75mW/cm^2) at 24h post-injection, and tumor growth was recorded daily. Even at such a higher dose, conjugate **4** did not show any significant photosensitizing efficacy. Under similar treatment parameters conjugates **1–3** and **5** were also evaluated. Interestingly, compounds **2** and **5** produced minimal tumor-response, whereas the mice injected with **1** and **3** on exposing with light produced 100% mortality. This could be possibly due to high singlet oxygen formation in organs such as liver and spleen (due to high uptake of conjugates) on exposing the tumor (which is in close proximity to tumors) with the light. However at the same imaging dose (10 μmol/kg), but at a lower light dose, compared to **3** the conjugate **1** [HPPH-3Gd(III)aminobenzyl DTPA] was quite effective in both RIF and Colon 26 tumor models. The best tumor response was obtained on exposing the tumors with a laser light (665 nm at 70 J/cm^2, 70 mW/cm^2) at 24h post treatment (Figure 8).

In vivo biodistribution of HPPH-3Gd(III)ADTPA conjugate—The biodistribution of HPPH-3Gd(III)ADTPA conjugate was evaluated *in vivo* using Ward tumors in Fischer 344 rats. The distribution of the conjugate to tumor was higher than blood, muscle, heart, lung, spleen, stomach and intestine, and similar to that of liver (Figure 9). However, kidney showed a significant uptake of the conjugate at 24 hours, with a considerable decrease seen at 48h post injection, suggesting glomerular filtration of the conjugate by the kidneys.

Toxicological Study (a range finding study)—For a fourteen-day range-finding toxicity study, male and female SD rats (3 per sex per group) were treated with vehicle (phosphate buffered saline), 5, 10 and 25 μmol HPPH-3Gd(III)ADTPA/kg (a total of 24 rats). The lowest dose chosen coincided with lowest dose required for MR imaging efficacy, and the upper dose was five times that. Higher doses could not be obtained because of solubility limitations. No infusional toxicities were seen, and the rats showed no acute toxicities. As is standard in single dose studies, the rats were sacrificed 14 days after treatment.

Full hematological and serum chemistry evaluation was conducted on an individual animal basis at the time of necropsy, and histopathological evaluation of all major organs (20 tissues per rat) were carried out. Representative toxicological results in tissues of an animal that received 25μmol/kg (2.5× higher than the imaging/therapeutic dose) are shown in Figure 10. H&E results obtained from liver, spleen, kidney, skin, heart and lungs following HPPH-3Gd (III)ADTPA administration demonstrated that each tissue appeared normal, well-preserved and devoid of toxicological lesions.

DISCUSSION

With advances in the early detection of cancerous lesions, highly localized therapies such as photodynamic therapy present a favorable alternative to invasive surgery or systemic chemotherapy. In this paper, we report the advancement of combined MR contrast/PDT agents. The combination of diagnostic and therapeutic efficacy into a single compound offers multiple advantages. In the case of deep seated tumors, the ability to use non-invasive imaging to better delineate tumor boundaries or metastatic spread immediately prior to or during PDT would be a valuable tool to the clinician. Furthermore, the inclusion of MR contrast enhancing groups into the therapeutic agent provides a probe to determine intratumoral concentration of the PDT agent. To a first approximation, the T_1 relaxation rate (R_1) of tissue increases linearly with contrast agent concentration within the tissue (20). Therefore, measuring baseline relaxation rates and monitoring the increase in R_1 allows for individualized measurements of the pharmacokinetics of the agent within the tumor. In the past, the time requirements for *in vivo* T_1 relaxometry were prohibitive for routine assessment of changes in T_1 rates. However, through rapid measurement techniques, T_1 rates can be measured well under 5 minutes in a patient (21–23). These advances, as well as the lack of non-ionizing radiation associated with MRI, allow for serial assessment of multifunctional agent concentration. Thus, light dosing parameters may potentially be adjusted on a per patient basis, maximizing efficacy while reducing phototoxicity to surrounding normal tissue. Furthermore, if these multifunctional agents can be modified for more effective uptake into tumors, MRI may be used serially to measure individual tumor uptake at variable time points, and PDT treatment can begin as soon as intratumoral levels reach a pre-determined threshold.

As determined by T_1 relaxometry, there was minimal uptake in muscle at 24 hours post injection. Biodistribution studies of ^{14}C labeled compound displayed similar preferential uptake of HPPH-3Gd(III)ADTPA in the tumor. Using the relaxivity 13.50 $(mM \cdot s)^{-1}$ for HPPH- 3Gd(III)ADTPA (as determined *in vitro*), mean tumor concentration of the conjugate at 24 hours was 9.0 μM. The primary cause of preferential tumor accumulation is believed to be the result of the enhanced permeability and retention effect associated with tumor vasculature. It has been reported that Gadophrin-2, another porphyrin-based compound, binds with the serum protein albumin and accumulates preferentially in the rim of necrotic regions (24,25).

At the MR imaging dose (10 μmol/kg) the utility of the conjugate **1** was also investigated for *in vivo* fluorescence imaging and PDT. As can be seen from Figures 7 and 8 the conjugate produced significant tumor contrast and long-term PDT activity in two tumor models. However, HPPH-3Gd(III)ADTPA produced excellent PDT response and tumor-imaging potential at lower doses as well (data not shown). The difference between the MR imaging dose required for HPPH-Gd(III)ADTPA is 10-to 20-fold less than the clinical MR imaging agent Gd(III)-DTPA in mice and rat models. This study further indicates that the conjugates in which tumor-avid photosensitizer (HPPH) was used as a vehicle to MR imaging requires much higher dose than required for fluorescence imaging and therapy. However, even at higher doses required for MR imaging, no histologic evidence of toxicity was seen by detailed *in vivo* organ toxicological studies in rats. Thus, the development of such multifunctional conjugates with tumor-avid photosensitizer presents a clear potential for a “see and treat” approach in photodynamic therapy.

CONCLUSION

In summary, our study indicates that tumor-avid photosensitizers can be used as vehicles to deliver the desired imaging agent to tumor. The presence of three Gd(III)ADTPA moieties increased tumor conspicuity during MR imaging while maintaining anti-tumor PDT efficacy.

The fluorescent characteristic of the HPPH-based conjugate (Ex: 665 nm, Em: 715 nm) also showed a great potential for complementary optical imaging of the tumor. Thus, the HPPH-3Gd (III)ADTPA as a single moiety can be used for tumor imaging by MR and fluorescence with an option of photodynamic therapy. Our next goal is to increase the tumor specificity of these multifunctional agents by introducing variable number of tumor-targeting moieties such as: a) cyclic RGD peptide which binds preferably to the a_vb_3 integrin expressed in the neoangiogenic vasculatures of tumors *(267, 27)*, b) folic acid to target folate receptors known for their high expressions in breast cancers and c) certain β-galactosides for binding to integrin-3 to target metastatic brain tumors. A target-specific approach may help to reduce the dose required for MR imaging efficacy, which is already 10-fold less than that of the typical dose of Gd-DTPA (100 μmol/kg) used clinically.

Supplementary Material

Refer to Web version on PubMed Central for supplementary material.

Acknowledgments

The authors are highly thankful to Dr. Peter Kanter for animal toxicological studies, Dr. Toth, Pathologist (RPCI) for analyzing the *in vivo* toxicological data and to Dr. Rustum (Chair, Department of Cancer Biology) for valuable discussions. Financial support from the NIH (Grants R21/33 CA109914 and PO1, CA55791), Roswell Park Alliance Foundation and the shared resources of the RPCI Support Grant (P30CA16056) is highly appreciated.

REFERENCES CITED

1. Dougherty TJ, Gomer CJ, Henderson BW, Jori G, Kessel D, Korbelik M, Moan J, Peng Q. Photodynamic therapy. J Natl Cancer Inst 1998;90:889–905. [PubMed: 9637138]
2. Overholt BF, Wang KK, Burdick JS, Lightdale CJ, Kimmey M, Nava HR, Sivak MV Jr, Nishioka N, Barr H, Marcon N, Pedrosa M, Bronner MP, Grace M, Depot M. Five-year efficacy and safety of photodynamic therapy with photofrin in barrett's high-grade dysplasia. Gastrointest Endosc 2007;66:460–468. [PubMed: 17643436]
3. Yamaguchi S, Tsuda H, Takemori M, Nakata S, Nishimura S, Kawamura N, Hanioka K, Inoue T, Nishimura R. Photodynamic therapy for cervical intraepithelial neoplasia. Oncology 2005;69:110–116. [PubMed: 16118506]
4. Loewen GM, Pandey R, Bellnier D, Henderson B, Dougherty T. Endobronchial photodynamic therapy for lung cancer. Lasers Surg Med 2006;38:364–370. [PubMed: 16788932]
5. Nseyo UO, DeHaven J, Dougherty TJ, Potter WR, Merrill DL, Lundahl SL, Lamm DL. Photodynamic therapy (PDT) in the treatment of patients with resistant superficial bladder cancer: A long-term experience. J Clin Laser Med Surg 1998;16:61–68. [PubMed: 9728133]
6. Dolmans DE, Fukumura D, Jain RK. Photodynamic therapy for cancer. Nat Rev Cancer 2003;3:380–387. [PubMed: 12724736]
7. Sibata CH, Colussi VC, Oleinick NL, Kinsella TJ. Photodynamic therapy in oncology. Expert Opin Pharmacother 2001;2:917–927. [PubMed: 11585008]
8. Dougherty TJ, Pandey RK, Nava HR, Smith JA, Douglass HO, Edge SB, Bellnier D, O'Malley L, Cooper M. Preliminary clinical data on a new photodynamic therapy photosensitizer: 2-[1-hexyloxyethyl]-2-devinylpyropheophorbide-a (HPPH) for treatment of obstructive esophageal cancer. Proc SPIE 2000;3909:25–27.
9. Bellnier D, Greco W, Loewen G, Nava H, Oseroff A, Pandey R, Tsuchida T, Dougherty T. Population pharmacokinetics of the photodynamic therapy agent 2-[1-hexyloxyethyl]-2-devinyl pyropheophorbide-a in cancer patients. Cancer Res 2003;63:1806–1813. [PubMed: 12702566]
10. Jäger HR, Taylor MN, Theodossy T, Hopper C. MR imaging-guided interstitial photodynamic laser therapy for advanced head and neck tumors. Am J Neuroradiol 2005;26:1193–1200. [PubMed: 15891183]

11. Eljamel MS, Goodman C, Moseley H. ALA and photofrin® fluorescence-guided resection and repetitive PDT in glioblastoma multiforme: A single centre phase III randomised controlled trial. Lasers Med Sci 2008;23:361–367. [PubMed: 17926079]
12. Zilidis G, Aziz F, Telara S, Eljamel MS. Fluorescence image-guided surgery and repetitive photodynamic therapy in brain metastatic malignant melanoma. Photodiagn Photodyn Ther 2008;5:264–266.
13. Tanimoto A, Nakashima J, Kohno H, Shinmoto H, Kuribayashi S. Prostate cancer screening: The clinical value of diffusion-weighted imaging and dynamic MR imaging in combination with T2-weighted imaging. J Magn Reson Imaging I 2007;25:146–152.
14. Yuh W, Fisher D, Nguyen H, Tali E, Mayr N. The application of contrast agents in the evaluation of neoplasms of the central nervous system. Top Magn Reson Imaging 1992;4:1–6. [PubMed: 1419031]
15. Safir J, Zito J, Gershwind M, Faegenburg D, Tobin C, Cayea P, Wortman W, Sclafani L, Maurer V. Contrast-enhanced breast MRI for cancer detection using a commercially available system--a perspective. Clin Imaging 1998;22:162–179. [PubMed: 9559228]
16. Ward J. New MR techniques for the detection of liver metastases. Cancer Imaging 2006;6:33–42. [PubMed: 16766267]
17. Sakuma H. Magnetic resonance imaging for ischemic heart disease. J Magn Reson Imaging 2007;26:3–13. [PubMed: 17659549]
18. Runge VM, Muroff LR, Jinkins JR. Central nervous system: Review of clinical use of contrast media. Top Magn Reson Imaging 2001;12:231–263. [PubMed: 11687713]
19. Li G, Slansky A, Dobhal MP, Goswami LN, Graham A, Chen Y, Kanter P, Alberico RA, Spernyak J, Morgan J, Mazurchuk R, Oseroff A, Grossman Z, Pandey RK. Chlorophyll-a analogues conjugated with aminobenzyl-DTPA as potential bifunctional agents for magnetic resonance imaging and photodynamic therapy. Bioconjugate Chem 2005;16:32–42.
20. Shuter B, Wang S, Roche J, Briggs G, Pope JM. Relaxivity of Gd-EOB-DTPA in the normal and biliary obstructed guinea pig. J Magn Reson Imaging 1998;8:853–861. [PubMed: 9702887]
21. Schmitt P, Griswold MA, Jakob PM, Kotas M, Gulani V, Flentje M, Haase A. Inversion recovery TrueFISP: Quantification of T1, T 2, and spin density. Magn Reson Med 2004;51:661–667. [PubMed: 15065237]
22. Bellamy DD, Pereira RS, McKenzie CA, Prato FS, Drost DJ, Sykes J, Wisenberg G. Gd-DTPA bolus tracking in the myocardium using T1 fast acquisition relaxation mapping (T1 FARM). Magn Reson Med 2001;46:555–564. [PubMed: 11550249]
23. Cheng HM, Wright GA. Rapid high-resolution T1 mapping by variable flip angles: Accurate and precise measurements in the presence of radiofrequency field inhomogeneity. Magn Reson Med 2006;55:566–574. [PubMed: 16450365]
24. Ni Y, Marchal G, Yu J, Lukito G, Petre C, Wevers M, Baert AL, Ebert W, Hilger CS, Maier FK. Localization of metalloporphyrin-induced “specific” enhancement in experimental liver tumors: Comparison of magnetic resonance imaging, microangiographic, and histologic findings. Acad Radiol 1995;2:687–699. [PubMed: 9419626]
25. Hofmann B, Bogdanov A Jr, Marecos E, Ebert W, Semmler W, Weissleder R. Mechanism of gadophrin-2 accumulation in tumor necrosis. J Magn Reson Imaging 1999;9:336–341. [PubMed: 10077034]
26. Brooks PC, Clark RA, Cheresh DA. Requirement of vascular integrin alpha v beta 3 for angiogenesis. Science 1994;79:1157–1164.
27. Anderson SA, Rader RK, Westlin WF, Null C, Jackson D, Lanza GM, Wickline SA, Kotyk JJ. Magnetic resonance contrast enhancement neovasculature with a(v)β3-targeted nanoparticles. Magn Reson Med 2000;44:433–439. [PubMed: 10975896]

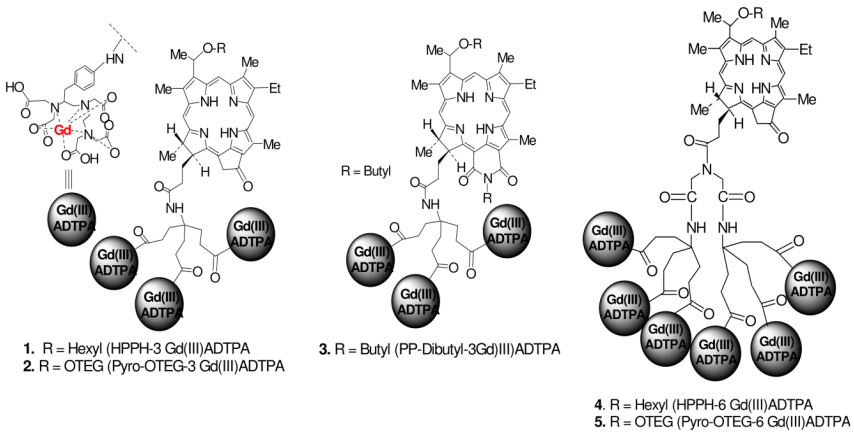

Figure 1.
Gd(III)ADTPA conjugates of photosensitizers with variable lipophilicity

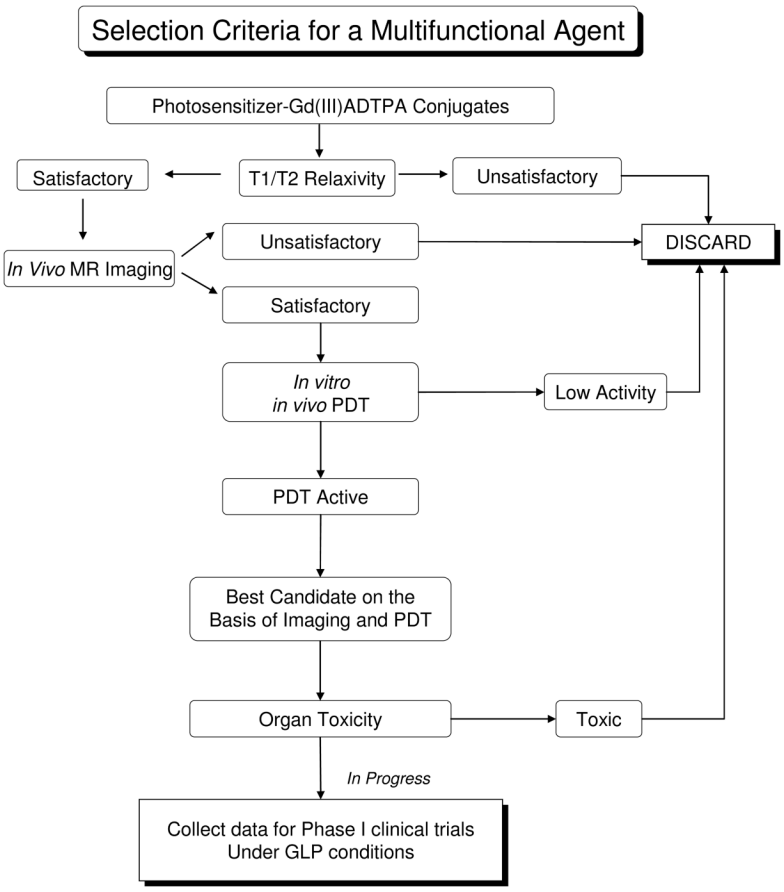

Figure 2.
Selection criteria for identifying the best candidate for MR imaging and therapy.

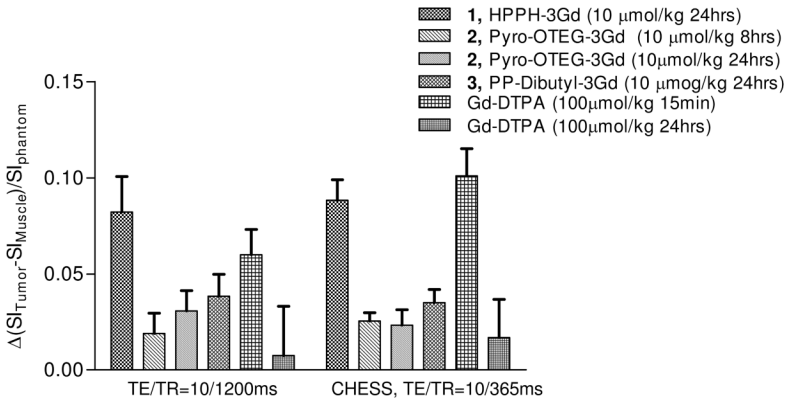

Figure 3.

Comparison of the relative increases in contrast between tumor and back muscle for the MR contrast/PDT agents and a clinical dose of Gd(III)-DTPA. The tumor-to-muscle-contrast enhancement caused by the HPPH-3Gd(III)ADTPA (10 μmol/kg) was comparable to the enhancement from clinical Gd(III)-DTPA (100 μmol/kg) seen immediately after injections, despite HPPH-3Gd(III)ADTPA being administered at one-tenth the concentration of Gd(III)-DTPA, and imaged 24 hours post injection.

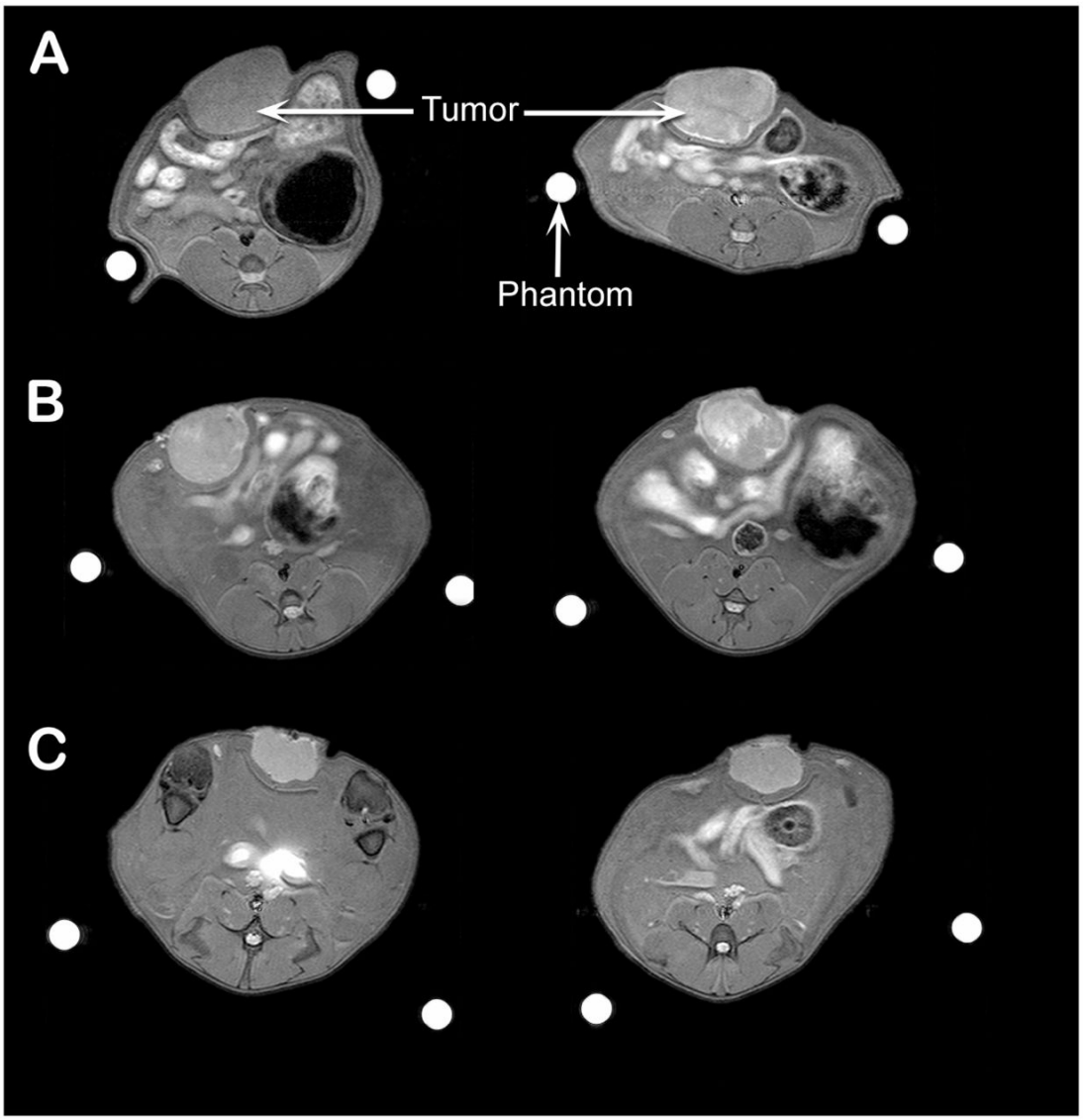

Figure 4.
A visible increase in signal intensity was seen in rat Ward Colon tumors (arrow) from pre-injection (left) to post-injection (right, 24 hrs post-injection) of conjugate **1** (HPPH-3Gd) at 10 μmol/kg (A) and at 5 μmol/kg (B). Tumor contrast enhancement of HPPH-3Gd compares favorable to Gd-DTPA administered at 10 μmol/kg (C) at 24h postinjection.

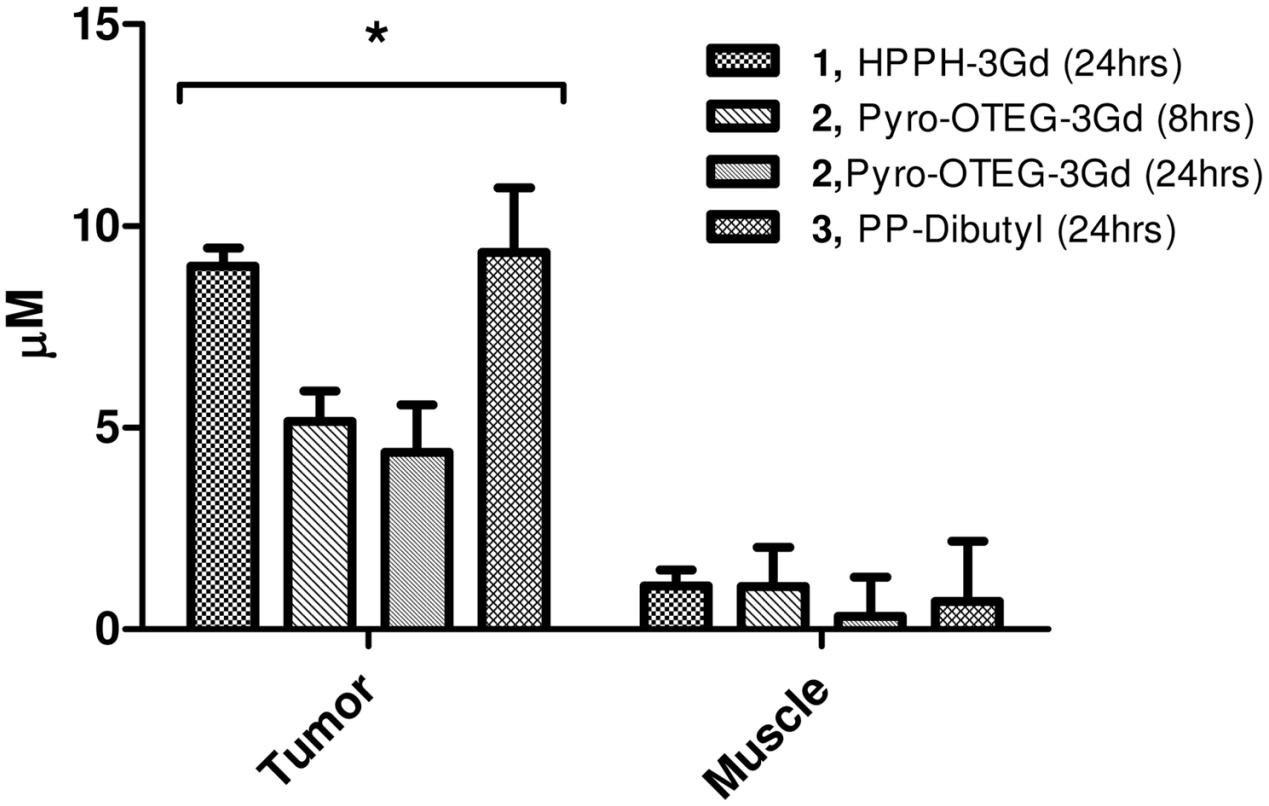

Figure 5.

Preferential tumor uptake of multifunctional agents was seen 24 hours post administration as compared to muscle (dose = 10 μmol/kg of each conjugate). Concentrations of agents were determined by dividing by change in T_1 relaxation rate by the relaxivity of each agent as determined *in vitro.* Each compound showed a statistically greater amount of uptake in the tumor as compared to muscle (* $p<0.05$, unpaired Student's t-test.)

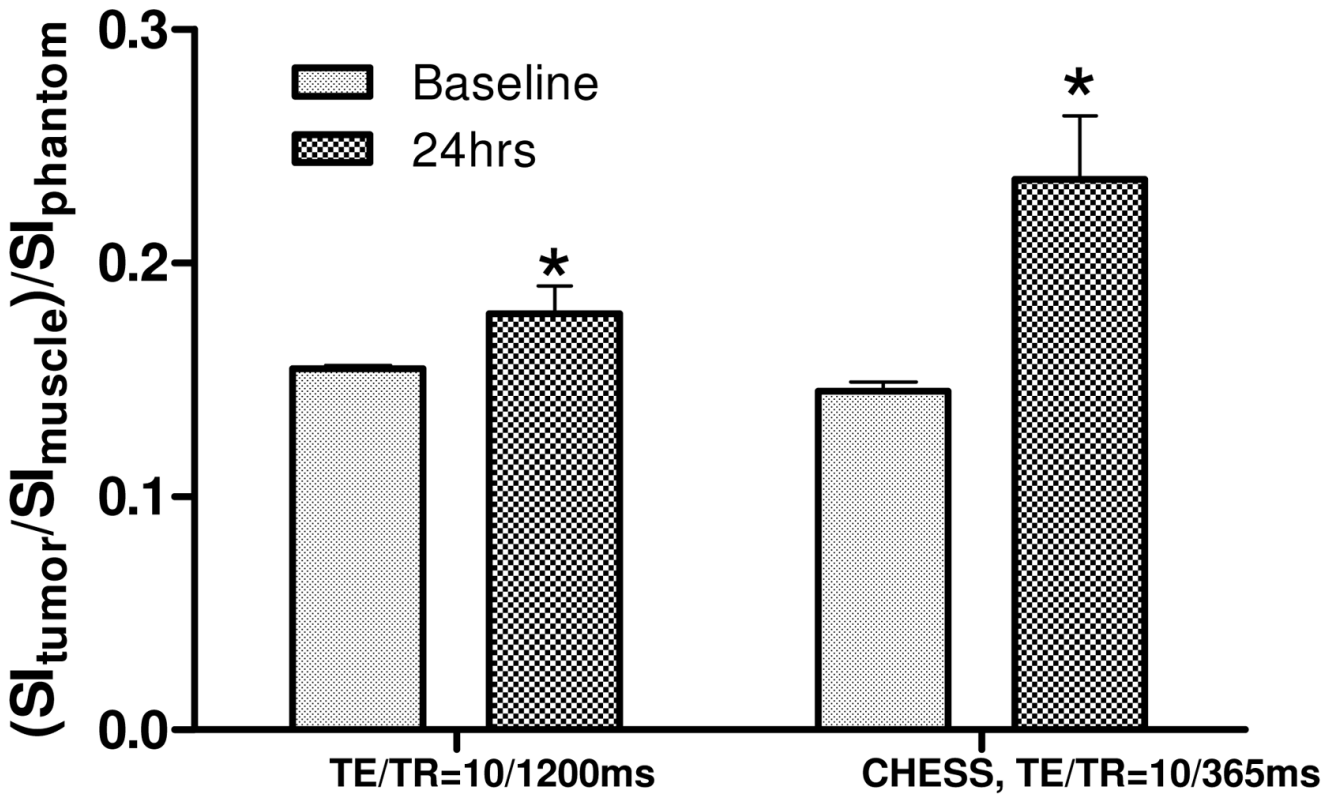

Figure 6.
Increase in contrast between RIF tumor and leg muscle was significant for conjugate **1**, HPPH-3Gd (dose=10 μmol/kg; * $p<0.05$, paired, one-way Student's t-test.)

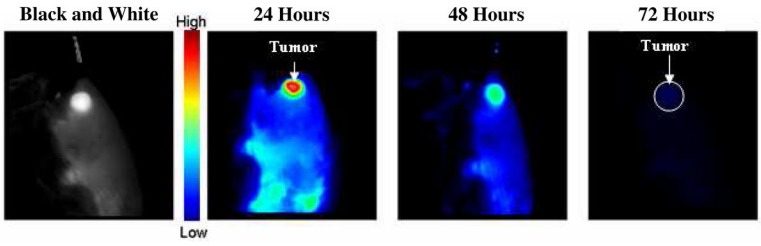

Figure 7.
In vivo fluorescent images of conjugate **1** (HPPH-3Gd) in BALB/c mice at 24, 48 and 72 hours with an imaging/therapeutic dose of 10 μmol/kg. Spectrally unmixed images are presented with a false color representing fluorescence intensity of the imaging agent. Best tumor-images were obtained at 24h post injection. A pre-analysis black and white image at 24 hours is given for comparison with the false color images provided.

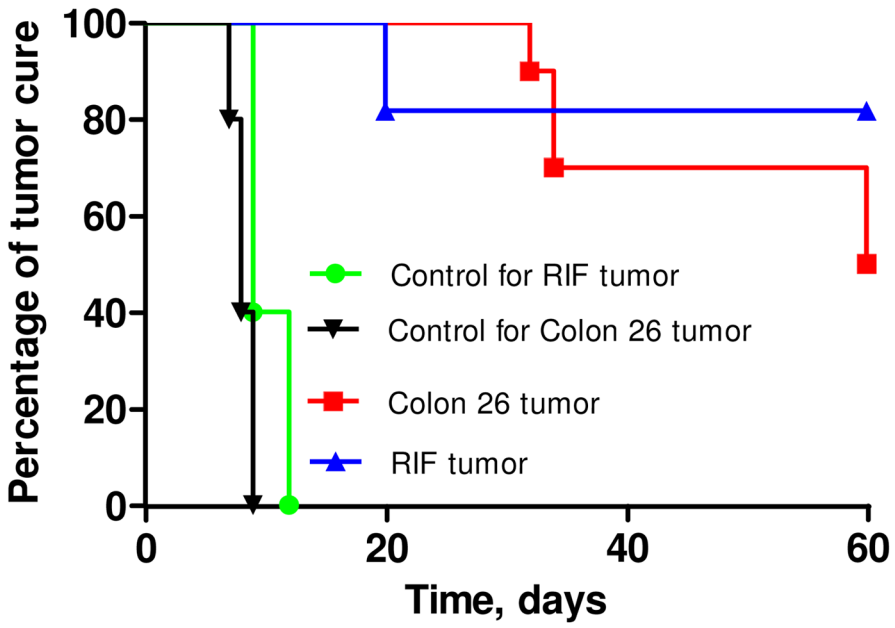

Figure 8.
In vivo PDT efficacy of HPPH-3GD(III)ADTPA **1** in (**A**) C3H mice bearing RIF tumors and (**B**) BALB/c mice bearing Colon 26 tumors at an imaging dose (10 μmol/kg). Mice were irradiated with a laser light (70 J/cm^2, 70 mW/cm^2) and the tumor size was measured daily.

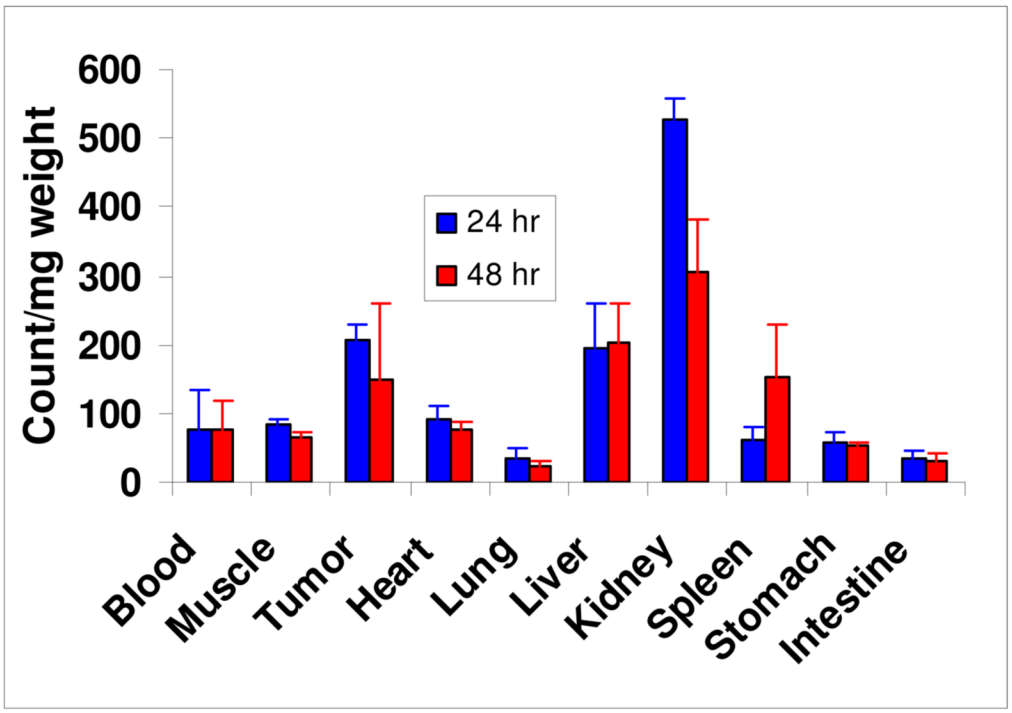

Figure 9.

The *in vivo* biodistribution of ^{14}C-labeled HPPH-3Gd(III)ADTPA in Ward colon tumors (3 rats/group): The ^{14}C-labeled conjugate (0.2 mL/0.8μCi) was administered to 3 rats/group. At 24 and 48 h after injection, 3 rats/time point were sacrificed. Preferable uptake of conjugate **1** in the tumor was seen at 24 and 48 hours compared to most normal tissues.

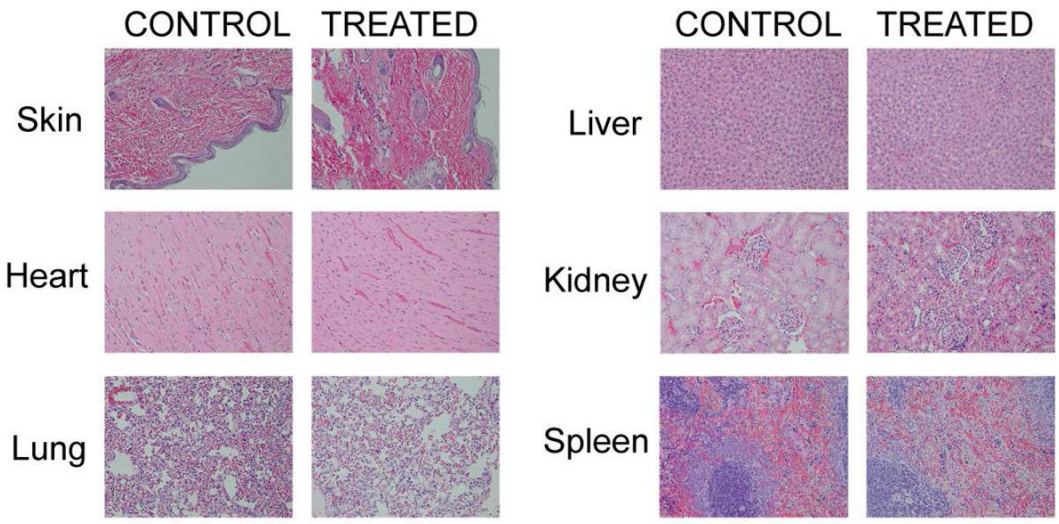

Figure 10.

In vivo histochemical staining of HPPH-3Gd(III)-ADTPA conjugate. No histologic evidence of toxicity was observed in the animals (rats) administered with HPPH-3Gd(III)-ADTPA at a dose of 25 μmol/kg (2.5-fold higher than the imaging dose). Histological structure of every organ was preserved.

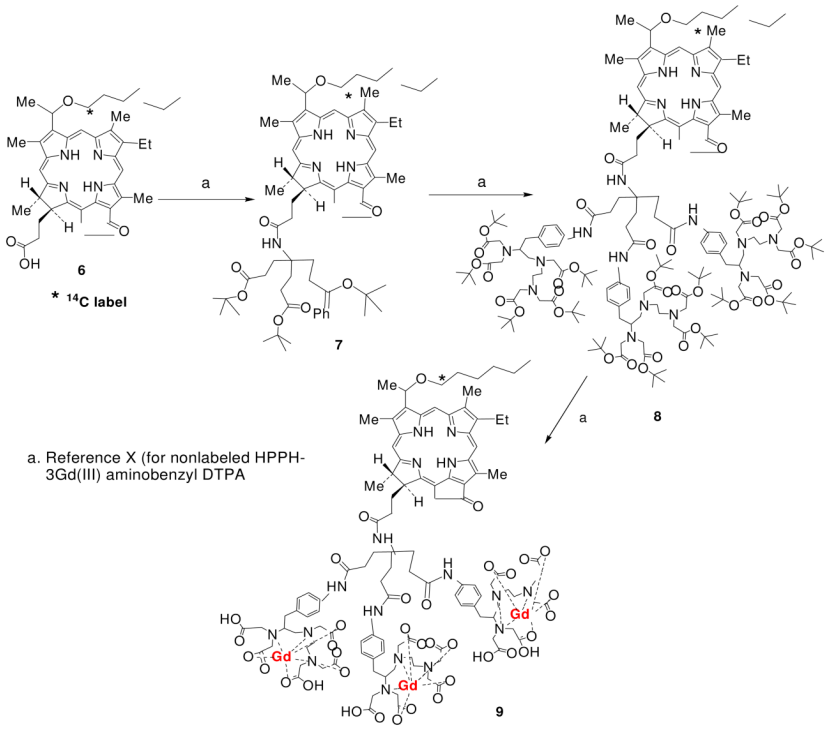

Scheme 1.
Synthesis of ^{14}C-labeled HPPH-3Gd(III)ADTPA

Table 1

Dose dependence of HPPH-3Gd(III) ADTPA on increase in contrast and T_1 relaxation rate.

Scan Protocol	10 μmols/kg	5 μmols/kg	2.5 μmols/kg
TE/TR = 10/1200ms (%increase of contrast)	101.5	40.1	−2.71
CHESS Fat Saturation (% increase of contrast)	130.3	51.4	8.60
ΔR_1 $(s)^{-1}$	0.12	0.08	0.05